RESTRICTED INVESTIGATION REPORT 1639R

CSIRO

INSTITUTE OF ENERGY AND EARTH RESOURCES

DIVISION OF MINERAL PHYSICS AND MINERALOGY

GEOLOGICAL STRUCTURE AND MAGNETIC SIGNATURES OF HAMERSLEY BIFS

D.A. CLARK AND P.W. SCHMIDT

AMIRA PROJECT 78/P96B: APPLICATIONS OF ROCK MAGNETISM

P.O. Box 136
NORTH RYDE, NSW
AUSTRALIA 2113

JUNE 1986

CSIRO

INSTITUTE OF ENERGY AND EARTH RESOURCES

DIVISION OF MINERAL PHYSICS AND MINERALOGY

POLICY ON RESTRICTED INVESTIGATION REPORTS

Restricted Investigation Reports issued by this Division deal with projects where CSIRO has been granted privileged access to research material. In return for this access, they provide recipients with an opportunity to take advantage of results obtained on their samples or problems. Initially, circulation of Restricted Investigation Reports is strictly controlled, and we treat them as confidential documents at this stage. They should not be quoted publicly, but may be referred to as a "personal communication" from the author(s) if my approval is sought and given beforehand.

The results embodied in a Restricted Investigation Report may eventually form part of a more widely circulated CSIRO publication. Agreements with sponsors or companies generally specify that drafts will be first submitted for their approval, to ensure that proprietary information of a confidential nature is not inadvertently included.

After a certain period of time, the confidentiality of particular Restricted Investigation Reports will no longer be an important issue. It may then be appropriate for CSIRO to announce the titles of such reports, and to allow inspection and copying by other persons. This procedure would disseminate information about CSIRO research more widely to Industry. However, it will not be applicable to all Restricted Investigation Reports. Proprietary interests of various kinds may require an extended period of confidentiality. Premature release of Restricted Investigation Reports arising from continuing collaborative projects (especially AMIRA projects) may also be undesirable, and a separate policy exists in such cases.

You are invited to express an opinion about the security status of the enclosed Restricted Investigation Report. Unless I hear to the contrary, I will assume that in eighteen months time I have your permission to place this Restricted Investigation Report on open file, when it will be generally available to interested persons for reading, making notes, or photocopying, as desired.

B.J. Embleton
CHIEF OF DIVISION

Distribution List

	Copy No.
CRAE	1 - 5
CSIRO Division of Mineral Physics and Mineralogy	
D.A. Clark	6
P.W. Schmidt	7
B.J.J. Embleton	8
CSIRO IEER Records	9 - 12

This is copy number 7 of 12.

CONTENTS

	Page
SUMMARY	1
1. INTRODUCTION	3
2. PRINCIPLES OF MODELLING	3
3. COMPLICATING FACTORS	7
4. MODELLING THE TURNER SYNCLINE	10
5. ACKNOWLEDGEMENTS	15
6. REFERENCES	16
APPENDIX I	17

LIST OF FIGURES

Fig. 1. Equivalent dipping sheets which produce an identical anomaly.

Fig. 2. Anomaly due to the anisotropic component of induced magnetisation.

Fig. 3. Anomaly due to the isotropic component of induced magnetisation.

Fig. 4. Anomaly due to post-folding remanence.

Fig. 5. Anomaly due to pre-folding remanence over a syncline.

Fig. 6. Anomalies associated with pre-folding and post-folding remanences over a thin anticlinal bed.

Fig. 7. Anomalies due to pre-folding and post-folding remanences over a thick anticlinal bed.

Fig. 8. Anomaly due to anisotropic component on induced magnetisation over an anticline.

Fig. 9. Preliminary model for SW limb of Turner syncline (cf profile 1310)

Fig. 10. Preliminary model for SW limb of Turner syncline (cf profiles 1350 and 1400)

Fig. 11. Preliminary model for the NW limb of the Turner syncline (cf profiles 1270 and 1342)

Fig. 12. Preliminary model for the SE limb of the Turner syncline (cf profiles 1580, 1600 and 1650).

SUMMARY

The characteristic magnetic signatures observed over the Turner syncline can be explained on the basis of the measured magnetic properties and the known geological structure. Successful modelling of the BIFs requires consideration of the following factors:

(i) The high intrinsic anisotropy of the BIFs. The induced magnetisation can be separated into an isotropic component (which is dominant for most rocks) and an anisotropic component (which is important for BIFs). The dip dependence of the associated anomalies is quite different for the two components and this explains some previously enigmatic features of the observed anomalies.

(ii) The presence of a significant sub-horizontal remanence, which is dominantly pre-folding in areas of low metamorphic grade but which appears to be post-folding in the Turner syncline. The strike-dependence of the effective Q is of crucial importance to correct interpretation.

Principles of interpretation are outlined and illustrated with theoretical examples. Preliminary models for the SW,NW and SE limbs of the Turner syncline are presented. These models point the way to detailed interpretation of the magnetics over the syncline.

Various complications which may affect interpretation are discussed. The effects of variable elevation (draping) are clearly evident in the data and we outline a method for modelling this. The difference between measured anomalies (ΔB_m) and the theoretical "total field" anomaly (ΔB_T), which is calculated by all published algorithms, is stressed and we give a method for directly modelling the measured anomaly. We find that the difference between the two quantities is clearly detectable for the intense anomalies over BIFs, although the general shape of the anomalies does not differ markedly.

We also discuss the effects of non-uniform demagnetising fields and interactions between adjacent BIF units. We conclude that these perturbations are relatively minor and do not justify the much greater effort required for their computation. We also recommend modification of

modelling programs to allow bodies with variable strike, not orthogonal to the profile, to be treated. This is essential for modelling a profile over both limbs of the Turner syncline, particularly given the strike-dependence of the contribution of remanence to the anomaly.

The palaeomagnetic and petrophysical studies described in an earlier report have provided the key to understanding the magnetic pattern over the Turner syncline. The experience gained from detailed modelling of the mapped structures should enable magnetics over buried structures to be interpreted with much greater confidence.

1. INTRODUCTION

This study was prompted by the puzzling nature of the observed magnetic anomalies over BIF units with known structure. The classical dip dependence of anomaly shape was not observed for the north and south limbs of the Turner and Brockman synclines, for instance. Failure to understand the magnetic pattern over areas of known structure precludes use of magnetics to interpret the structure of buried units and greatly degrades the utility of the aeromagnetic surveys as indicators of structural settings which are thought to favour ore formation.

Resolution of this problem was hindered formerly by lack of knowledge of the magnetic properties of the BIFs. This has been largely remedied by the palaeomagnetic and petrophysical studies described in the Restricted Investigation Report 1638R (Clark and Schmidt, 1986). With this information and with suitable algorithms for calculating anomalies due to remanently magnetised anisotropic 2D bodies considerable insight into the observed magnetic signatures over the Turner syncline has been gained. We feel that rapid progress in understanding the magnetic response of the BIFs will proceed from detailed modelling of anomalies over mapped structures along the lines of the preliminary modelling which is described below. This should then allow the magnetics over other areas to be interpreted with much greater confidence.

2. PRINCIPLES OF MODELLING

Although most of the principles noted here and in the next section are either obvious or are well known from published work it is considered useful to summarise them so they may be readily referred to during the subsequent discussion. For the most part our attention is restricted to bodies of great strike extent. Tectonic tilting is considered to have occurred by rotation about strike i.e. we neglect fold axis plunge and non-cylindrical folding.

(i) For 2D bodies the component of magnetisation directed along strike makes no contribution to the anomaly. The component of magnetisation in the orthogonal plane (the vertical plane containing the

principal profile) is hereafter referred to as the effective magnetisation. The effective field is defined analogously. It follows that a high Koenigsberger ratio does not necessarily imply a dominant contribution of remanent magnetisation to the anomaly.

The effective Q is strike-dependent and in fact a strong sub-horizontal remanence has negligible effect when directed along strike, irrespective of any tectonic tilting.

(ii) The effective remanence may be divided into two categories: Pre-folding components (such as early diagenetic CRM), which rotate with the beds during folding, and post-folding components (e.g. VRM) which are independent of bedding attitude (Clark, 1983 and Appendix I). The magnetic expression of these two types of remanence is different. In a given rock unit both types may be present. Metamorphic overprints may be acquired either before or after folding. A remanence acquired syndeformationally causes a response equivalent to a complex remanence with pre-folding and post-folding components. Strong anisotropy can produce a similar result.

(iii) The effective induced magnetisation of a BIF may be divided into an isotropic component equal to $k_{\perp}\tilde{F}_{eff}$ and an anisotropic component which is confined to the bedding plane and which has magnitude $(k_{=}-k_{\perp})F_{=}$, where $\tilde{F}_{eff}$ is the effective field and $F_{=}$ is the component of the effective field which lies in the bedding plane (i.e. the down-dip component of $\tilde{F}$). This is equivalent to dividing the susceptibility matrix K into an isotropic component $k_{\perp}I$ and an anisotropic component $(K-k_{\perp}I)$ which has an anisotropy ratio of infinity. The parameters $k_{=}$ and $k_{\perp}$ represent <u>apparent</u> susceptibilities (i.e. they include the effects of self-demagnetisation of the BIF unit as a whole) parallel and perpendicular to bedding respectively.

(iv) The isotropic component of induced magnetisation is parallel to the ambient field and its intensity is independent of bedding attitude. The anisotropic component rotates with the beds i.e. it behaves similarly to pre-folding remanence, but with the difference that its intensity

varies with dip. As the beds tilt towards orthogonality with the effective field the intensity of the anisotropic component decreases to zero and, with further tilting, changes sign i.e. the direction reverses.

(v) The dip of a 2D sheet-like body of great depth extent cannot be determined from its anomaly without knowledge of the direction of the effective magnetisation. This is because of a fundamental ambiguity between dip and the effective inclination of a 2D semi-infinite dipping sheet with a flat top. Equivalent sheets, producing identical anomalies, are characterised by a constant angle between the effective magnetisation and the plane of the sheet and by a constant value of the product of the effective magnetisation intensity and the orthogonal thickness (refer to Fig. 1). This relationship may be expressed alternatively: as a dipping sheet and its effective magnetisation rotate together the anomaly shape remains unchanged and the anomaly amplitude varies as the sine of the dip.

(vi) Points (ii) and (v) imply that the shape of the anomaly arising from pre-folding remanence is independent of the dip of the sheet. It follows that if the effective magnetisation is overwhelmingly dominated by pre-folding remanence the dip cannot be determined from the observed anomaly.

(vii) Points (iv) and (v) imply that the shape of the anomaly arising from the induced magnetisation of a highly anisotropic unit essentially depends on whether the dip (measured from the end of the principal profile closest to MN) is shallower or steeper than the plane normal to the effective field (the sign of the anomaly being opposite for the two cases). This point is illustrated in Fig. 2. Thus if the effective Q is much less than unity the dip of a highly anisotropic unit can only be interpreted as shallower or steeper than this reference plane and cannot be quantitatively estimated. However, this information may be quite useful in some circumstances.

(viii) From (ii), (iv) and (v) it follows that the anomaly arising from the isotropic induced component and post-folding remanence (refer to Fig. 3 and Fig. 4 respectively) is sensitive to dip. In favorable circumstances, given knowledge of the post-folding remanence (obtained directly from sampling or inferred from modelling mapped structures with varying strikes and dips), dips can be interpreted from anomalies.

(ix) Magnetic anomalies are not very sensitive to the depth extent of a body, provided it is several times the depth to the top plus the height of the sensor. It is therefore reasonable to represent the limbs of most synclines and anticlines by dipping sheets of infinite depth extent. The parameters which can be interpreted from the anomalies are: the depth to the top, the breadth of the top (provided it is comparable to or greater than the depth plus sensor height) and (given knowledge of the magnetisation) the dip or (given the dip) the effective magnetisation.

(x) Since the two limbs of a syncline are generally well separated the anomalies associated with each limb are virtually independent and may be interpreted separately, at least in a preliminary analysis. When a horizontal unit with a stable remanence is folded to form a syncline the two limbs represent opposite ends of the original horizontal sheet, for which the edge effect anomalies are opposite in sign. It follows from this and point (vi) above that the anomaly associated with pre-folding remanence has opposite sign for the two limbs of a syncline. This is illustrated in Fig. 5.

(xi) On the other hand anomalies due to anticlines are superpositions of the anomalies due to adjacent limbs. This has some interesting consequences. It can be easily shown from (v) that the anomaly arising from a thin anticlinal bed (represented by two thin sheets) with isotropic induced magnetisation ± post-folding remanence is identical to that produced by a single thin sheet, with the same magnetisation direction, which bisects the two limbs. For the same structure pre-folding remanence produces no anomaly and anisotropic induced magnetisation produces a relatively weak anomaly. As the thickness of the folded bed increases the anomaly associated with pre-folding remanence becomes significant and exhibits a distinctive signature: an antisymmetric anomaly with reversed polarity. These points are illustrated in Fig. 6 and Fig. 7. Fig. 8 illustrates the anomaly associated with anisotropic induced magnetisation of a symmetric anticline with an eroded crest for a range of dips of the limbs.

3. COMPLICATING FACTORS

A number of possible complications, some applicable to the specific environment (intense magnetisations and large anomalies) and some of more general relevance to interpretation, were examined.

(xii) All published algorithms (e.g. the Talwani algorithms) calculate the "total field anomaly" as the projection of the anomalous field vector onto a fixed direction in space (the direction of the regional geomagnetic field F). This is the quantity referred to as ΔB_T by Emerson et al. (1985). However "total field" magnetometers actually measure the magnitude of the resultant magnetic field (the vector sum of the regional geomagnetic field and the local anomalous field). The magnitude of F is then subtracted from the readings to obtain ΔB_m, the measured total field anomaly (refer to Appendix I).

ΔB_m and ΔB_T differ because the direction of the resultant field changes near a magnetic body. If the anomalous field represents a significant perturbation of the geomagnetic field the two quantities may differ markedly. The maximum error in approximating ΔB_m by ΔB_T is $\sim (\Delta B)^2/2F$. Normally $\Delta B < 1000\gamma$, $F \simeq 50{,}000\gamma$ so that the difference is less than 1% of the anomaly, which is negligible. For an anomaly of $10{,}000\gamma$, however, the error is about 1000γ (10%) and for a $20{,}000\gamma$ anomaly the two quantities differ by 20%.

It is clear that attempts to model the very strong anomalies observed over BIFs by curve matching may produce significant errors if ΔB_T is calculated. There is a simple solution to this problem: ΔB_m should be calculated from the theoretical models and matched with observed anomalies. The required procedure is straightforward and is outlined below.

Emerson et al. (1985) presented formulae for a suite of magnetic models including the 2D flat-topped dipping sheet and sloping step. An arbitrary 2D body can be approximated by a body of polygonal cross-section which can be regarded as a superposition of sloping steps (with appropriate sign of the magnetisation). For convenience these formulae

are given in Appendix I, together with diagrams and notation. The formulae are general, allowing the computation of the anomalous field component along an arbitrary direction. In particular explicit expressions are given for ΔB_x, ΔB_y, ΔB_z and ΔB_T (components along the principal profile, along strike, vertically downwards and parallel to the regional geomagnetic field respectively).

The magnitude of the local (perturbed) field, F', is given by:

$$F' = [(F_x + \Delta B_x)^2 + (F_y + \Delta B_y)^2 + (F_z + \Delta B_z)^2]^{1/2}$$

where $F_x = F \cos\beta \cos I$, $F_y = F \sin\beta \cos I$, $F_z = F \sin I$.

The measured total field anomaly is then

$$\Delta B_m = F' - F$$

Note that for a composite source ΔB_m is not simply the superposition of ΔB_m anomalies due to individual bodies. It must therefore be calculated from the resultant anomaly components.

(xiii) Another consequence of the intense anomalies and high susceptibilities associated with the BIFs is that the magnetisation of homogeneous bodies is inhomogeneous because of a relatively strong, non-uniform, self-demagnetising field, which may represent a significant perturbation of the ambient field. Furthermore, anomalies arising from composite bodies are not simply the superposition of the anomalies due to the individual components, because of interactions between the components. In effect, each body is sitting in a perturbed field which may differ markedly from the regional geomagnetic field.

Eskola and Tervo (1980) have treated this problem and numerous calculations of anomalies due to highly magnetic composite bodies have been presented in the workshop proceedings edited by Hjelt and Phokin (1980). Calculation of the magnetisation and anomalous field requires numerical solution of an integral equation. Thus rigorous treatment of interactions in magnetics involves computation of similar nature to that required for EM modelling.

It is clear from the published work that the effects of interactions and inhomogenous demagnetising fields are negligible for susceptibilities below 0.1 G/Oe. Errors due to neglecting interactions between adjacent bodies of susceptibility 0.1 - 0.2 G/Oe are only a few per cent of the total anomaly amplitude and can therefore be ignored for most practical purposes. Thus interactions between BIF units can be safely ignored. Interactions are important, however, for massive magnetite deposits. The first order demagnetisation correction, assuming a uniform demagnetising field, is sufficiently accurate for the present purpose.

(xiv) It is usual in magnetic interpretation to assume a constant sensor height. In practice, survey profiles are often "draped" over the topographic relief in order to improve resolution of anomalies over topographically low areas.

Draped surveys are commonly believed to suppress topographic effects associated with magnetic terrain, but Grauch and Campbell (1984) have shown that this is a fallacy. Although the topography of the Turner syncline is not particularly rugged, it is conceivable that the observed anomalies are distorted relative to those that would be measured at constant elevation, given the highly magnetic nature of the hill crests, which rise about 300m above the surrounding plain, and the fact that the sensor probably is below the hill tops midway between the limbs. Although crests are oxidised relative to fresh BIF, intensities of magnetisation remain high and the crests cannot be ignored.

Given the location, elevation and terrain clearance from flight records it is not difficult to model anomalies along the flight profiles. We consider a profile consisting of a series of sloping linear segments chosen to approximate the actual profile. As a model we take the 2D body of polygonal cross-section (MAGMOD X of Appendix IV). Let the j^{th} vertex of the piecewise linear profile have co-ordinates (X_j, Z_j) and let δ_j be the slope of the segment joining the j^{th} and $(j + 1)^{th}$ vertices (measured positive downwards from the horizontal line passing through (X_j, Z_j)). The co-ordinates of the i^{th} corner of the polygonal model are (x_i, z_i) with respect to a horizontal profile passing through the (arbitrary) origin (refer to Fig. A1). The co-ordinates with respect to the j^{th} segment of the profile are then

$$x_{ij} = x'_j + (X_j - x_i)\cos\delta_j + (Z_j - z_i)\sin\delta_j$$

$$z_{ij} = -(x_i - X_j)\sin\delta_j + (z_i - Z_j)\cos\delta_j$$

where $\delta_j = \tan^{-1}[(Z_{j+i} - Z_j) / (X_{j+1} - X_j)]$ and x'_j is the distance along the j^{th} segment of the profile.

Substitution of the new co-ordinates into the formula for MAGMOD X yields the theoretical anomaly along that segment of the profile. The anomaly can be plotted as a function of the profile co-ordinate x' (the total distance along the profile, measured from (x_1, z_1)),

where $x' = x'_j + \Sigma(X_{k+1} - X_k)\sec\delta_k$ (the summation being from k=1 to k=j-1). Alternatively, if the flight records are on file the anomaly can be calculated at successive points on the profile using the co-ordinates directly.

(xv) Attempts to model the Turner syncline were complicated by the differing strikes of the north and south limbs when they are intersected by single profiles. It is therefore desirable to introduce flexibility into the modelling of 2D bodies by allowing calculation of theoretical anomalies along an arbitrary traverse, not restricted to be perpendicular to strike. The correction is very straightforward: if Θ is the angle between the traverse and the principal profile a distance x along the traverse corresponds to $x\cos\Theta$ along the principal profile.

4. MODELLING THE TURNER SYNCLINE

Preliminary interpretation of the aeromagnetics over the Turner syncline was aided by the information on the magnetic properties of the BIFs, by the geological mapping, by a previous palaeomagnetic study by Schmidt and Embleton (1985) and by mapping of the metamorphic grade throughout the Hamersley basin by Smith et al. (1982).

The NRM of BIFs from areas of relatively low metamorphic grade can be assumed to be pre-folding, with unfolded direction (dec = 314^o, inc = -5^o), as at Wittenoom and Paraburdoo. In areas of higher metamorphic grade, such as

the Turner syncline, it is possible that the NRM is predominantly a metamorphic overprint of Ophthalmian age. This hypothesised post-folding remanence is assumed to be parallel to the dominant overprint found in the Mt Jope volcanics, which were deformed in the Ophthalmian orogeny. The overprint direction is dec = 304°, inc = -19° (Schmidt and Embleton, 1985).

Modelling was used in an attempt to define the nature of the remanence carried by the BIFs in the Turner syncline. Obviously discrimination between the in situ directions of these magnetisations is very difficult if either the beds are flat-lying or the strike of the fold structures is approximately NW. A range of dips and strikes allows the effects of tectonic tilting on remanence to be evaluated and distinguished from the effects of induced magnetisation.

The most perplexing feature of the magnetics over the Turner syncline is the occurrence of prominent highs over the northward dipping SW limb as well as over the southward dipping NW limb. There is also a change of the magnetic signature along strike, the highs being fairly broad and symmetrical to the west, becoming more sharply peaked with very steep gradients on the southern flank as we move eastwards. Profiles 1310 and 1350 represent these two signatures respectively.

The qualitative similarity of the magnetic signatures over the NW and SW limbs of the syncline is inconsistent with the effective magnetisaion being dominated either by the isotropic induced component or by post-folding remanence because of the strong dip-dependence of the anomaly arising from such components (refer to (viii) above). In particular the isotropic induced component would give rise to a symmetric high over the northern limb and an antisymmetric anomaly with a prominent low to the south over the southern limb.

If the effective magnetisation is dominated by pre-folding remanence a signature similar to that shown in Fig. 5 would be observed, which is clearly not the case. Thus by elimination the anomaly over the SW limb of the syncline must be predominantly due to the anisotropic component of the induced magnetisation. In this case the anomalies over the two limbs should be broadly similar in form, but not in amplitude (refer to point (vii) above), as is actually observed.

It therefore appears that the distinctive signature of the SW limb of the Turner syncline reflects the high anisotropy of the BIFs and the fact that the effective remanence (whether pre-folding, post-folding or composite) is small because the NRM is sub-parallel to the strike for this limb. For limbs with different strike the remanence may make a significant contribution (point (i) above). The anomaly amplitude is sensitive to the dip and will even change sign for limbs with shallow dip to the NE (point (vii) above). The anomaly over the SW limb is lower than for the southward dipping limb because $F_=$ is smaller for the SW limb.

A model which produces an anomaly qualitatively resembling that measured over the SW limb along profile 1310 as shown in Fig. 9. The strike and dip are based on the mapped geology. Topography and profile draping are ignored in this preliminary model. The Brockman and Weeli Wolli Formations are modelled as a single body because there is no separation of their anomalies evident in the data. The anomaly maximum is about 7,500γ and the difference between ΔB_m and ΔB_T is relatively small. It can be seen that ΔB_m has a less pronounced low to the south and this is a general feature of predominently positive anomalies. On the northern flank of the anomaly high the anomalous field vector is sub-parallel to the Earth's field and the difference is negligible.

Note that the theoretical anomaly remains positive to the north of the causative bodies. This is true of any model qualitatively resembling that shown. However the measured anomaly drops below the regional base level between the limbs of the syncline. We conclude that the broad low in the centre of the syncline is an artefact of the draping. This is supported by modelling of the northern limb which demonstrates that the apparent low is too extensive and too pronounced to be produced by the same bodies that give rise to the symmetric highs over the northern limb. The effect of draping over the southern limb is to steepen the gradient on the southern flank of the magnetic high. Because of the lack of information on the aircraft elevation we did not attempt to refine the models to obtain close fits to the measured anomalies.

The anomaly for this model is not very sensitive to the intensity of the remanence, but a high intrinsic anisotropy (~5) is required for the

more magnetic units (Brockman and Weeli Wolli formations). This anisotropy is within the plausible range, but lies towards its upper limit.

Assuming pre-folding remanence does not change the anomaly greatly but does appear to slightly reduce the resemblance to the measured profile, unless the dips are increased to about 80^{o}, which is significantly steeper than the dips mapped at the surface. This suggests that the NRM may be predominantly post-folding, but cannot be considered definitive.

Modelling of the sharper, more intense anomalies along strike requires all four BIFs to be treated as separate bodies because their separate effects are evident in the anomalies. A preliminary model which matches typical profiles (e.g. 1350 and 1400) quite well is shown in Fig. 10. The model could be refined by sub dividing the Brockman IF, as the effects of the Dales Gorge and Joffre members are discernable in several profiles (e.g. 1400 and 1411). Note that the modelled bodies are less magnetic than individual BIFs because of the intervening shale units (and mineralisation?)

The major differences between the models shown in Figs. 9 and 10 are a topographic effect and a probable change in apparent magnetisation of the Weeli Wolli formation along stike. The narrowness of the anomaly over the Brockman IF and the steepness of the gradients on its flanks imply that the sensor height above the source is somewhat less than the nominal terrain clearance of 200m. A good fit is obtained if it is assumed that in this region the aircraft cleared the prominent ridge representing the outcropping Brockman IF by only 100m. This seems plausible and should be checked with flight records. Because the aircraft cannot follow the terrain exactly the sensor height is likely to exceed the average terrain clearance immediately on either side of the ridge. This may account for the decrease in response over the Weeli Wolli formation as the topographic relief associated with the Brockman formation increases. It may also be significant that the outcrop expression of the WWF disappears in this area, suggesting a greater thickness of cover. Thus the apparent change in magnetic properties along strike may largely reflect geometry rather than geology.

A preliminary model for the NW limb is presented in Fig. 11. The theoretical anomaly does not match a particular profile but represents a crude compromise between typical profiles such as 1270 and 1342. The dip (50^{o}S) is a compromise value because the mapped dips at the surface would produce intersection of units at shallow depth if extrapolated to the subsurface. Again no attempt was made to refine the model because topography and flight path geometry are evident in the profile. The model assumes post-folding remanence but differences between this model and one which assumes pre-folding remanence are slight, and are certainly not diagnostic. This is because the effective remanences are not greatly dissimilar for the particular strike and dip of this limb.

The theoretical profile shows greater separation of anomalies associated with individual units than the observed profile, as well as an apparent shift with respect to the outcrop distribution. Better agreement would be obtained by displacing the sheets slightly and spacing them more closely, which is compatible with the subsurface distribution inferred from the mapped dips.

The anomalies over the SE limb of the syncline are particularly interesting because the change of strike with respect to the SW limb highlights the strike dependence of the effective remanence. The increased contribution of the remanence to the anomaly and the relative shallowness of the dip combine to produce a signature which is completely different to that of the SW limb.

Assuming an intrinsic anisotropy of 2-3 and a Koenigsberger ratio of ~1 and using the mapped dips of the Brockman and Boolgeda formations it is found that magnetic lows are developed over the BIFs, as shown in Fig. 12. If the remanence is assumed to be pre-folding the low is quite symmetric whereas a post-folding remanence produces an asymmetric low with a smaller high to the north. This latter anomaly qualitatively reproduces the response observed over the Brockman formation quite well (e.g. profiles 1580, 1600 and 1650), favouring the interpretation that the remanence is post-folding.

The Marra Mamba formation lies off the section shown and the Weeli Wolli formation only produces a small anomaly in this area, so these units were omitted from the model. The reduced response of the Weeli Wolli

formation may reflect deep weathering, as there is no outcrop mapped, and/or increased sensor height due to draping.

Another qualitative feature of the magnetics over the Turner syncline which can be explained by the magnetic properties is the pronounced high over the western tip of the structure, which is much more pronounced than the response over the eastern end. It is thought that this reflects the positive poles induced on the western side of the structure by the NNW directed remanence, enhancing the response due to positive poles induced on the upper surface. In the east negative poles are produced on the side of the structure, partially counteracting the effect of positive poles on the top surface.

The distinctive magnetic signatures found in different parts of the syncline and their explanation in terms of geological structure, using the knowledge gained from magnetic property measurements, demonstrates the potential of the magnetics for structural interpretation in unmapped areas. We therefore believe that this project can be regarding as highly successful in its fundamental aim of aiding interpretation through magnetic petrophysics.

5. ACKNOWLEDGEMENTS

Mr Bob Smith of CRAE first proposed this study. We would like to thank Bill Burns, John Ashley and Peter de Groot for explaining the problems of magnetic interpretation on the Hamersley Province. Our guides at Tom Price and Paraburdoo were Alex Mandyczewsky and Rod McKenzie respectively. We are grateful to them and to Richard Harmsworth for discussions on the geology of the iron ore and for the drill-core material, maps, logs and cross-sections which greatly simplified the task of unravelling our data. Dick Morris (CSIRO) explained aspects of the magnetite distribution in the BIFs.

6. REFERENCES

Clark, D.A., 1983. Comments on magnetic petrophysics. Bull. Aust. Soc. Explor. Geophys., 14, 49-62.

Clark, D.A. and Schmidt, P.W., 1986. Magnetic properties of the banded-iron formations of the Hamersley Group, W.A. Restric. Invest. Rep. 1638R, CSIRO Division of Mineral Physics and Mineralogy, Sydney.

Emerson, D.W., Clark, D.A. and Saul, S.J., 1985. Magnetic exploration models incorporating remanence, demagnetization and anisotropy: HP41C handheld computer algorithms. Explor. Geophys., 16, 1-122.

Eskola, L. and Tervo, T., 1980. Solving the magnetostatic field problem (a case of high susceptiblity) by means of the method of subsections. Geoexploration, 18, 79-95.

Grauch, V.J.S. and Campbell, D.L., 1984. Does draping aeromagnetic data reduce terrain-induced effects? Geophysics, 49, 75-80.

Hjelt, S.O. and Phokin, A.P., 1981. Interpretation of borehole magnetic data and some special problems of magnetometry. Dept. of Geophys., Univ. of Oulu, Finland, Rep. No. 1, 171 pp.

Schmidt, P.W. and Embleton, B.J.J., 1985. Pre-folding and overprint magnetic signatures in Precambrian (~2.9-2.7 Ga) igneous rocks from the Pilbara Craton and Hamerlsey Basin, N.W. Australia. J. Geophys. Res., 90, 2967-2984.

Smith, R.E., Perdrix, J.L. and Parks, T.C., 1982. Burial metamorphism in the Hamersley Basin, Western Australia. J. Petrology, 23, 75-102.

Appendix I Calculation of Anomalies due to Tilted Units. Effect of Tectonic Tilting on Pre-folding Remanence

Consider cylindrical folding about a horizontal axis. The strike direction closest to the horizontal projection of the remanence is selected and the dip is then defined to be positive (negative) if this strike direction goes from left to right (from right to let) as the observer faces the rock unit. If the unit is overturned the dip is >90°.

If the remanence direction with respect to the palaeohorizontal is (D,I), its related direction (D', I') is given by

$$D' = \tan^{-1} [\tan (D-STRIKE)\cos DIP - \tan I \sec(D-STRIKE) \sin DIP] + STRIKE$$

$$I' = \sin^{-1} [\sin I \cos DIP + \cos I \sin (D-STRIKE) \sin DIP]$$

SCHEMATIC RELATIONSHIP BETWEEN MEASURED, TRUE AND CALCULATED TOTAL MAGNETIC INTENSITY ANOMALIES

Southern hemisphere fields depicted with negative inclination

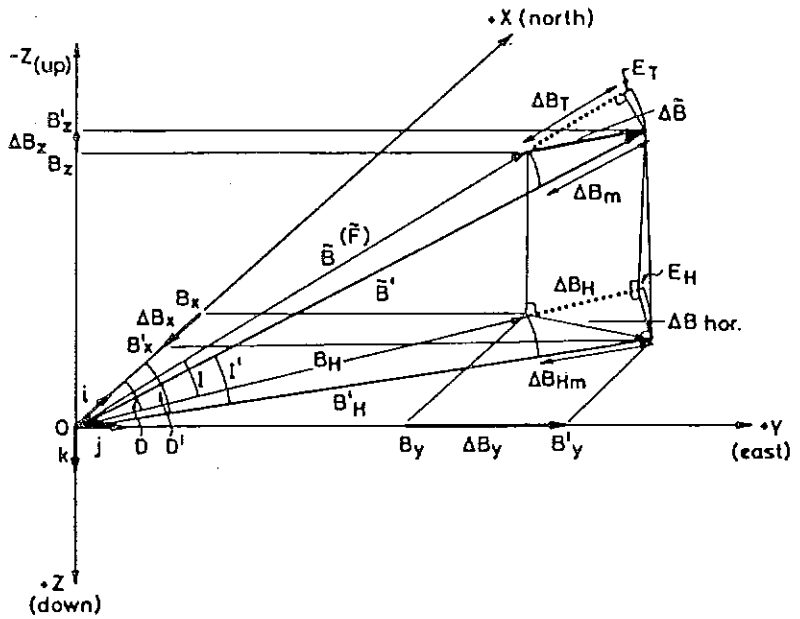

$\Delta B_T = \Delta B_H \cos I + \Delta B_z \sin I$ (computed total field anomaly)

$\Delta B_m = |\tilde{B}'| - |\tilde{B}|$ (measured total field anomaly)

$\Delta E_T = \Delta B_m - \Delta B_T = (|\Delta\tilde{B}|^2 - \Delta B_m^2)/2|\tilde{B}|$, $|\Delta\tilde{B}| \neq \Delta B_T \neq \Delta B_m$

θ (= D) is the angle between the +X axis and the horizontal projection of the field vector (ℓ,m,n)

$\tilde{i}$, $\tilde{j}$, $\tilde{k}$ unit vectors parallel to X, Y, Z axes respectively

ℓ, m, n direction cosines. For $\tilde{B}(F)$: $\ell = B_x/|\tilde{B}|$, $m = B_y/|\tilde{B}|$, $n = B_z/|\tilde{B}|$

$\ell\tilde{i} + m\tilde{j} + n\tilde{k}$ unit vector in direction (ℓ,m,n)

$\Delta\tilde{B}$ local magnetic anomaly vector, perturbing $\tilde{B}$

$\tilde{B}(\tilde{F})$ regional or "normal" magnetic field vector of Earth (constant over limited region)

$\tilde{B}'$ resultant (local) field = $\tilde{B} + \Delta\tilde{B}$; with declination D', inclination I'

ΔB_T component of $\Delta\tilde{B}$ along normal field $\tilde{B}$. This is the theoretical computed anomaly. Usually $\Delta B_T \approx \Delta B_m$

ΔB_m measured residual total field anomaly (scalar measurement of variation in magnitude of resultant field)

E_T departure of computed anomaly (ΔB_T) from measured anomaly (ΔB_m). Usually small

ΔB_{hor} horizontal projection of $\Delta\tilde{B}$ = true horizontal component of anomalous field

B_H component of $\tilde{B}(\tilde{F})$ along regional magnetic meridian

B_H' component of $\tilde{B}'$ along local anomalous magnetic meridian

ΔB_H computed horizontal field anomaly = component of $\Delta\tilde{B}$ along regional magnetic meridian

ΔB_{H_m} measured horizontal field anomaly $\Delta B_{H_m} = B_H' - B_H \neq \Delta B_{hor} \neq \Delta B_H$

$E_H = (\Delta B_H^2 - \Delta B_{H_m}^2)/2B_H = B_H'[1-\cos(D'-D)]$. Departure of computed from measured horizontal anomaly

ΔB_x true horizontal anomaly component along X axis = $B_x' - B_x$

ΔB_y true horizontal anomaly component along Y axis = $B_y' - B_y$

$\Delta B_{hor} = (\Delta B_x^2 + \Delta B_y^2)^{\frac{1}{2}}$

ΔB_z true vertical intensity anomaly, measured anomaly = vertical component.

ADDITION OF MAGNETIZATION VECTORS

$\tilde{J}$: [J, D, I]

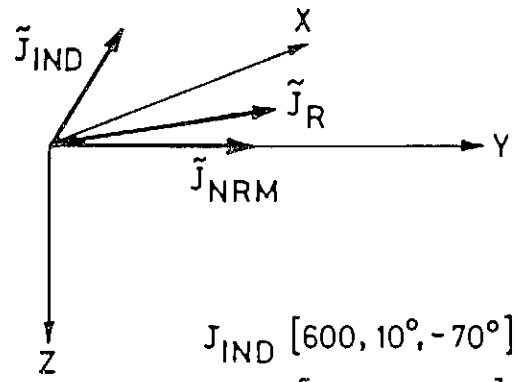

J_{IND} [600, 10°, -70°]

J_{NRM} [1000, 90°, 0°]

J_R [1196, 79°, -28°]

ANOMALOUS ΔB COMPONENTS IN VARIOUS DIRECTIONS

(l, m, n : direction cosines)

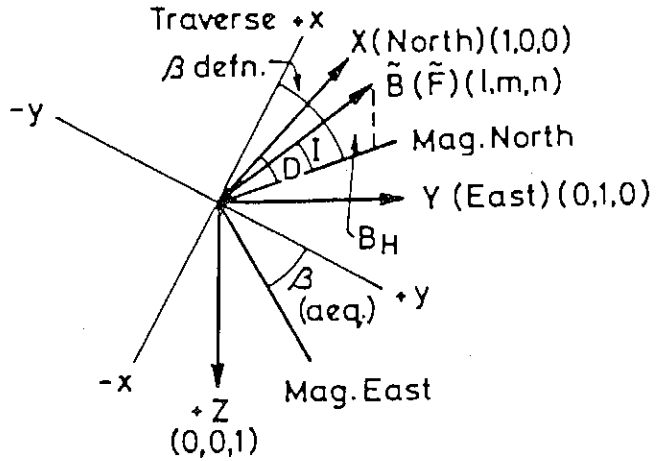

ERROR ARISING FROM ΔB_T APPROXIMATING ΔB_m

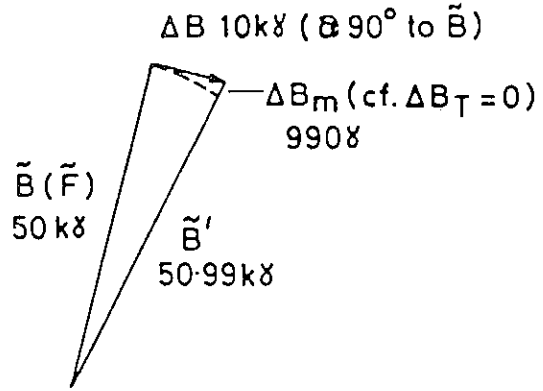

MAXIMUM DIFFERENCE BETWEEN ΔB_T AND ΔB_m WHEN $\Delta B_m = 0$

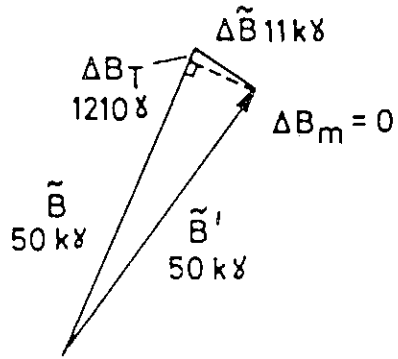

MAGNETIC MODELS

VII, VIII, IX

MAGNETIC MODEL

Note direction cosines ℓ,m,n ($\bar{F}$, Earth's field) and L,M,N (J_R, resultant magnetization) become (ℓ,o,n) and (L,O,N) in plane of section

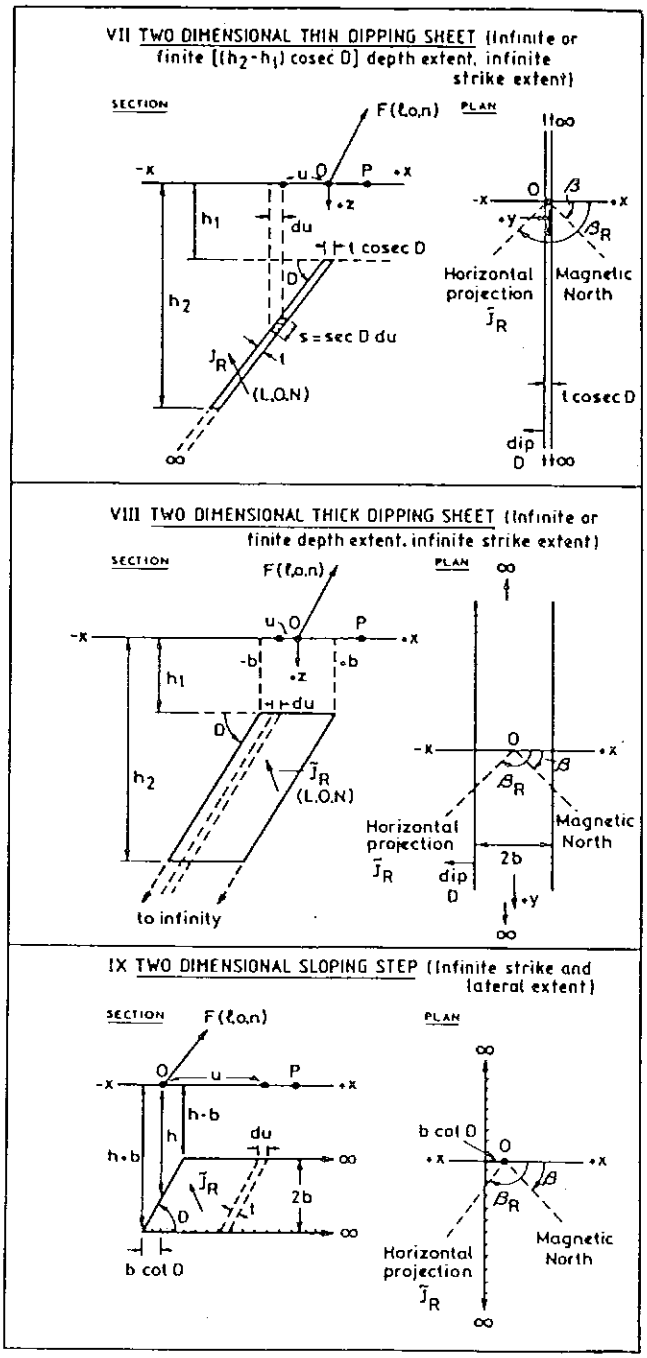

NOTATION (refer to MAGMOD diagrams and formulae)

O: origin of co-ordinates

x,y,x, Cartesian axes (right-handed)

S: surface area occupied by pole strength p ($=\pi R^2$ for plug radius R)

r: distance from fixed point of subsurface body to observation point, $r = (x^2+y^2+h^2)^{1/2}$.

h: vertical depth to fixed point of subsurface body

Y: half strike length (MAGMOD III)

X: half body width (MAGMOD III)

β: bearing of magnetic north, measured positive clockwise from the + x axis (the positive end of the principal profile).

β_R: bearing of the horizontal projection of the resultant magnetisation, measured positive clockwise from the + x axis.

$\tilde{F}$: Earth's magnetic field vector, with magnitude $|\tilde{F}|=F$, declination D (or bearing β) and inclination I (positive downwards)

$\tilde{J}$: magnetisation (contrast) vector

k: magnetic susceptibility (contrast)

$\tilde{J}_{IND}$: induced magnetisation vector

$J_{IND} = |\tilde{J}_{IND}|$, D, I: induced magnetisation magnitude, declination and inclination (neglecting demagnetisation)

$\tilde{J}_{NRM}$: remanent magnetisation vector, uncorrected for demagnetisation

$J_{NRM} = |\tilde{J}_{NRM}|$, D_{NRM}, I_{NRM}: remanent magnetisation magnitude, declination, inclination.

$\tilde{J}_R$: resultant magnetisation vector, uncorrected for demagnetisation ($\tilde{J}_R = \tilde{J}_{IND} + \tilde{J}_{NRM}$).

$J_R = |\tilde{J}_R|$, D_R, I_R: resultant magnetisation magnitude, declination, inclination

$\tilde{J}_R'$: resultant magnetisation vector, corrected for demagnetisation

$J_R' = |\tilde{J}_R'|$, D_R', I_R': demagnetisation-corrected resultant magnetisation magnitude, declination, inclination

p: magnetic pole strength

λ: line density of magnetic pole strength (pole strength per unit length)

σ: surface magnetic pole density (pole strength per unit area)

$\tilde{\mu} = \mu(L,M,N)$: magnetic dipole moment with magnitude μ and direction cosines L,M,N. $\mu = VJ$, where V is the volume of the causative body ($= 4\pi R^3/3$ if sphere) and J is magnetisation. magnitude.

$\tilde{\mu}_L = \mu_L(L,M,N)$: line density of magnetic dipole moment with magnitude μ_L and direction cosines L, M, N. $\mu_L = AJ$ (A = cross section area of the causative body).

$\tilde{\Delta B} = (\Delta B_x, \Delta B_y, \Delta B_z)$: anomalous magnetic field vector (assumed small compared to F for total field interpretation).

ΔB_i: magnetic anomaly component along measurement direction with direction cosines (ℓ', m', n') $i = z,x,y,H$ or T.

ΔB_H: horizontal magnetic anomaly (component of $\tilde{\Delta B}$ parallel to horizontal component of $\tilde{F}$).

ΔB_T: total field magnetic anomaly (component of $\tilde{\Delta B}$ parallel to $\tilde{F}$)

ℓ,m,n: direction cosines of $\tilde{F}$. $(\ell,m,n) = (\cos\beta\cos I, \sin\beta\cos I, \sin I)$

L,M,N: direction cosines of resultant magnetisation.
$(L,M,N) = (\cos\beta_R \cos I_R, \sin\beta_R \cos I_R, \sin I_R)$

ℓ',m',n': direction cosines of measurement direction

$(\ell',m',n') = (0,0,1)$ $(i=z)$

$= (1,0,0)$ $(i=x)$

$= (0,1,0)$ $(i=y)$

$= (\cos\beta,\sin\beta,0)$ $(i=H)$

$= (\cos\beta\cos I,\sin\beta\cos I,\sin I)$ $(i=T)$

d: (a) dip of thin or thick sheet measured downwards from -x axis
(b) dip of sloping step face measured downwards from -x axis

t: thickness of thin sheet

2b: (a) breadth of flat top of thick sheet
(b) vertical thickness of slab, away from sloping step face

MAGMOD VI, VII Semi-infinite thin sheet

General formula: $\Delta B_i = Jt\ [\frac{C_7 x+C_8 h}{x^2+h^2}]$

$\Delta B_i = \Delta B_z, \Delta B_x, \Delta B_y, \Delta B_H$ or ΔB_T

$C_7 = 2C_4 cosd+C_5 sind$; $C_8 = -2C_4 sind+C_5 cosd$

where C_4, C_5 are as for MAGMOD V

MAGMOD VIII Semi-infinite thick sheet

General formula: $\Delta B_i = Jsind\{(C_7/2)\ell n[\frac{(x+b)^2+h^2}{(x-b)^2+h^2}] + C_8[\tan^{-1}(\frac{x+b}{h}) - \tan^{-1}(\frac{x-b}{h})]\}$

$\Delta B_i = \Delta B_z, \Delta B_x, \Delta B_y, \Delta B_H$ or ΔB_T

C_7, C_8 are as for MAGMOD VII

MAGMOD IX 2D sloping step

General formula: $\Delta B_i = Jsind\{(C_7/2)\ell n[\frac{(x-bcotD)^2+(h-b)^2}{(x+bcotD)^2+(h+b)^2}] + C_8[\tan^{-1}(\frac{x-bcotD}{h}) - \tan^{-1}(\frac{x+bcotD}{h})]\}$

$\Delta B_i = \Delta B_z, \Delta B_x, \Delta B_y, \Delta B_H$ or ΔB_T

C_7, C_8 are as for MAGMOD VII

The response of finite dip extent or depth extent bodies is simply obtained by subtraction of the response of two bodies with infinite dip or depth extent.

MAGMOD X 2D body with polygonal cross-section

Magnetic anomalies are calculated by superposition of MAGMOD IX fields for N sloping steps. N vertices (x_j, z_j) are numbered in a clockwise sense from an arbitrary starting point. The steps make a negative contribution for increasing z and positive contribution for decreasing z. The position of the principal profile origin, x = 0, is arbitrary.

EQUATIONS (refer to MAGMOD IX; d = dip of step face)

$$j = 1 \text{ to } N-1: \Delta B_i = J \sin d_j \{(C_7/2)\ln[\frac{(x-x_{j+1})^2+z_{j+1}^2}{(x-x_j)^2+z_j^2}] + C_8[\tan^{-1}(\frac{x-x_{j+1}}{z_{j+1}}) - \tan^{-1}(\frac{x-x_j}{z_j})]\}$$

$$j = N: \Delta B_i = J \sin d_n \{(C_7/2)\ln[\frac{(x-x_1)^2+z_1^2}{(x-x_N)^2+z_N^2}] + C_8[\tan^{-1}(\frac{x-x_1}{z_1}) - \tan^{-1}(\frac{x-x_N}{z_N})]\}$$

$$d_j = \tan^{-1}(\frac{z_{j+1}-z_j}{x_j-x_{j+1}}) \text{ for } d_j\text{: } 0^0\text{-}90^0\text{; if } d_j \text{ negative, add } 180^0 \text{ (j=1 to N-1)}$$

$$d_N = \tan^{-1}(\frac{z_1-z_N}{x_N-x_1}) \text{ for } d_N\text{: } 0^0\text{-}90^0\text{; if } d_N \text{ negative, add } 180^0$$

MAGMOD X

TWO DIMENSIONAL BODY WITH POLYGONAL CROSS-SECTION

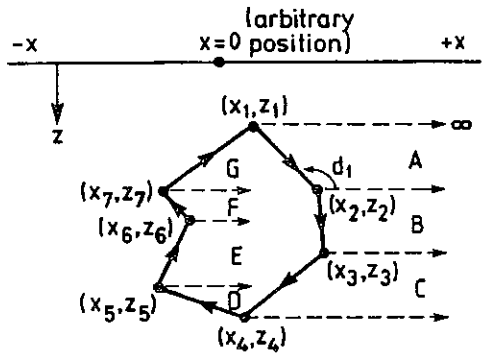

N vertices: (x_j, z_j)
N=7 here

Worked example MAGMOD X

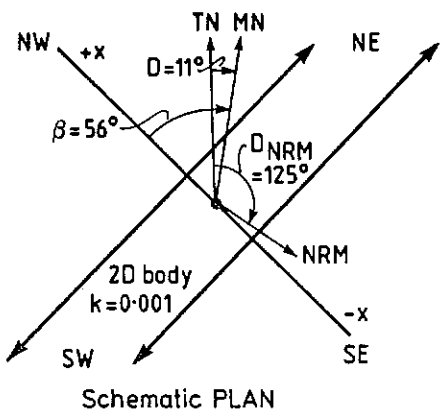

Schematic PLAN

IND. F = 58,000 γ (nT)
J = kF = 58 γ
I = -65°
D = 11°

NRM. J_{NRM} = 100 γ
I_{NRM} = 80°
D_{NRM} = 125°

RES. J_{RES} = 51·6 γ
I_{RES} = 62·8°
D_{RES} = 53·3°

ELEVATION (looking south west)

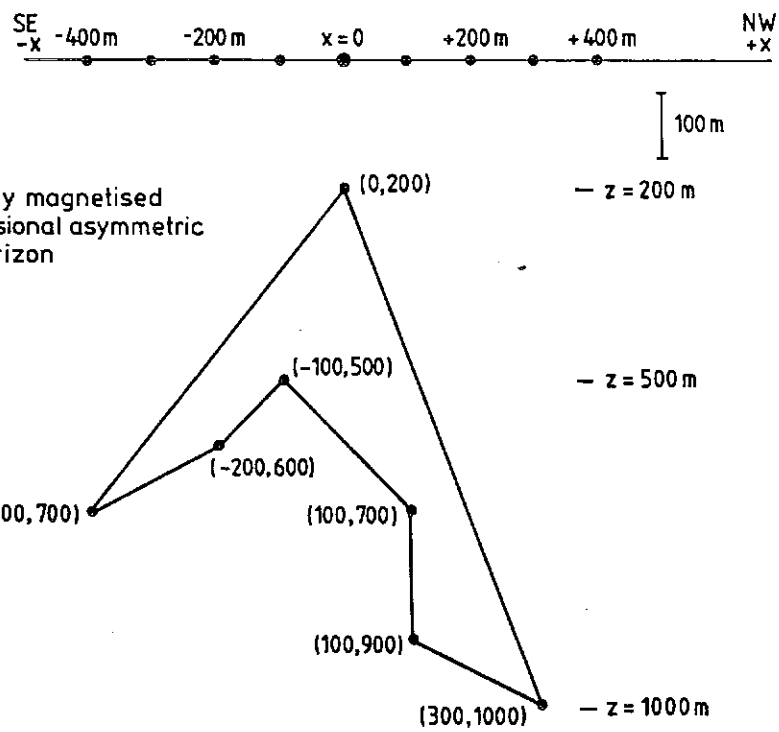

Remanently magnetised
two dimensional asymmetric
folded horizon
N = 7

GEOMETRY OF DRAPED PROFILE

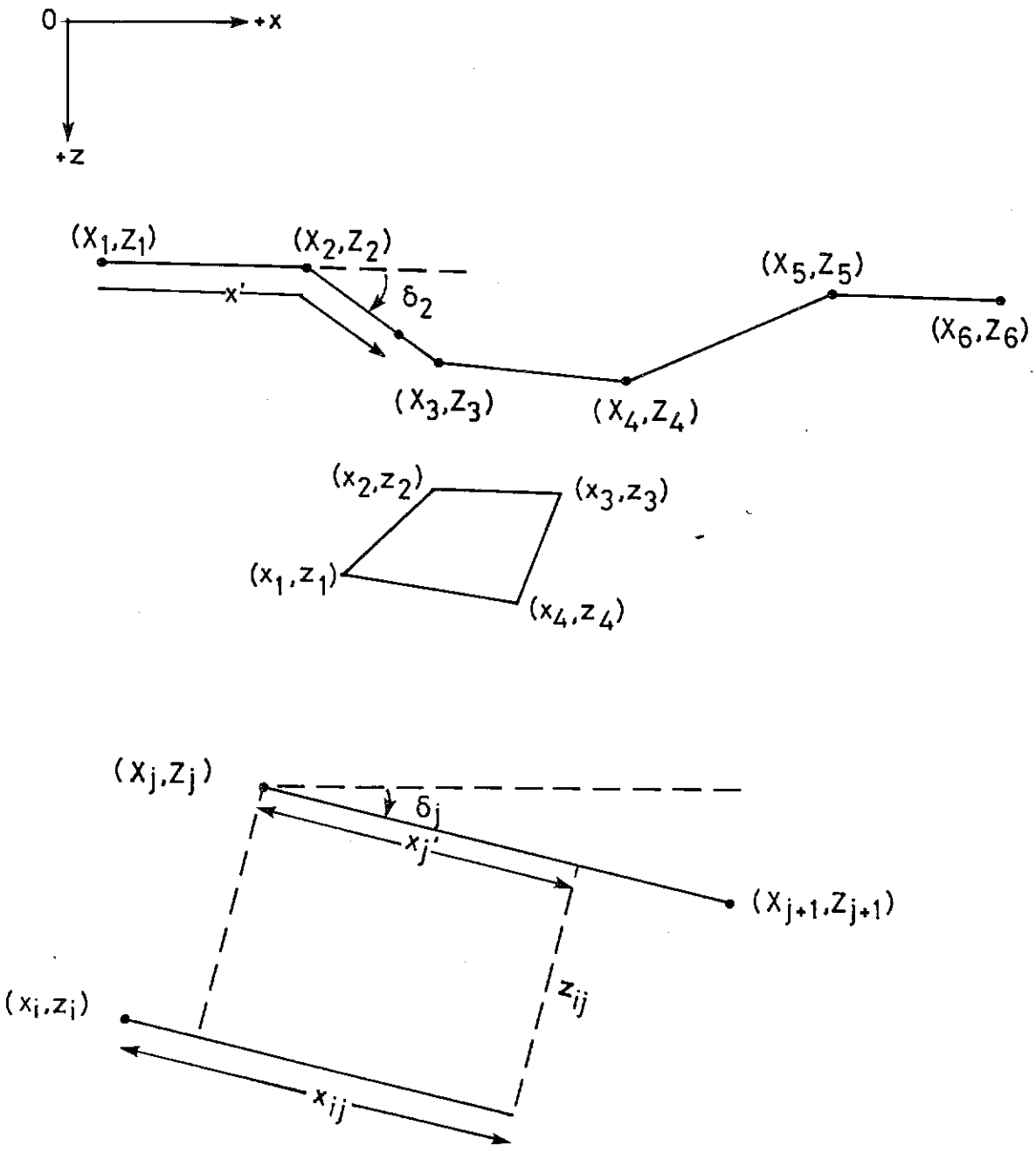

FIG.A1

Fig. 1 . Equivalent dipping sheets which produce an identical anomaly.

NON—UNIQUENESS

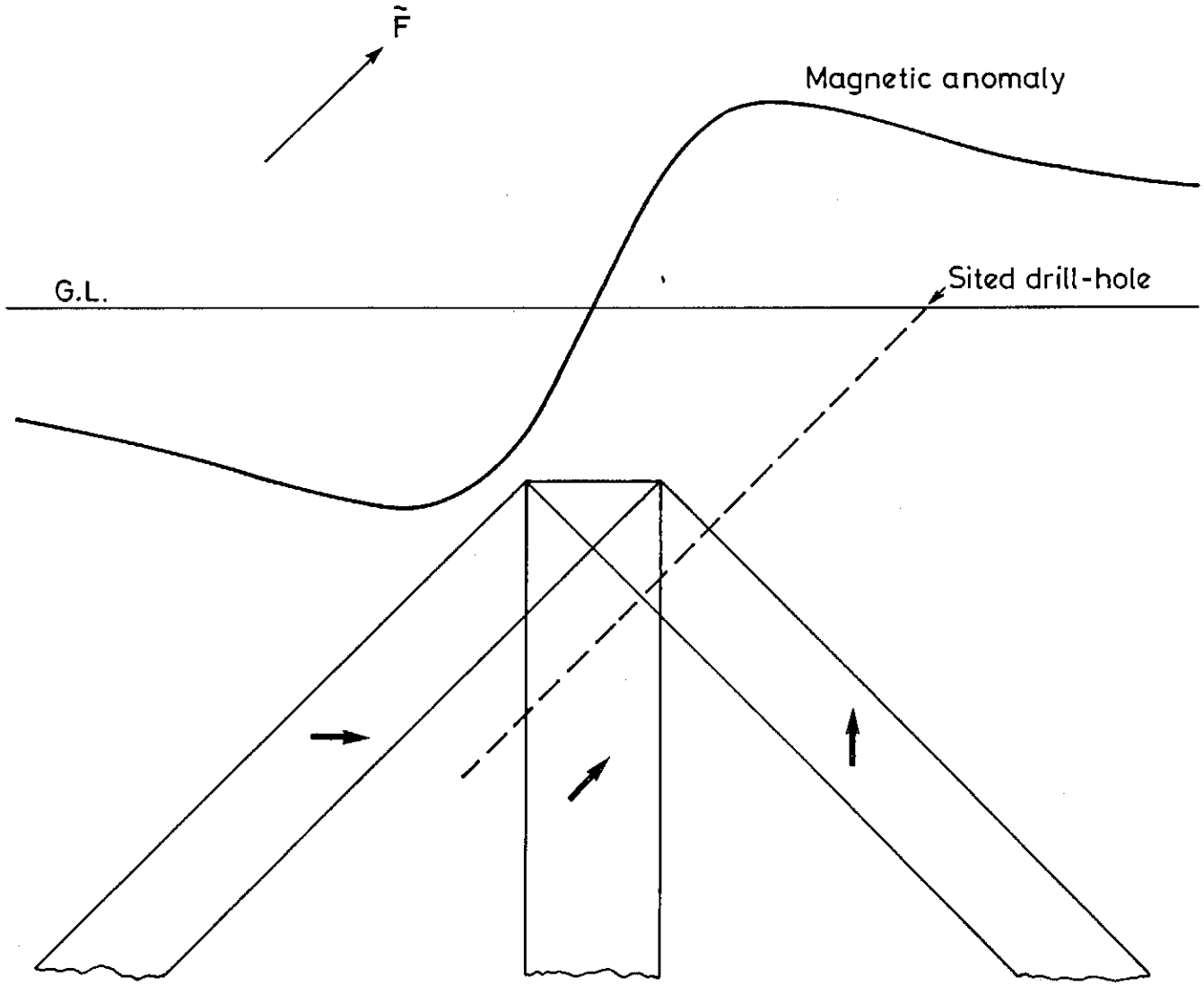

Fig. 2 . Anomaly due to the anisotropic component of induced magnetisation.

ANISOTROPIC DIPPING SHEETS (A=∞, Q=0)

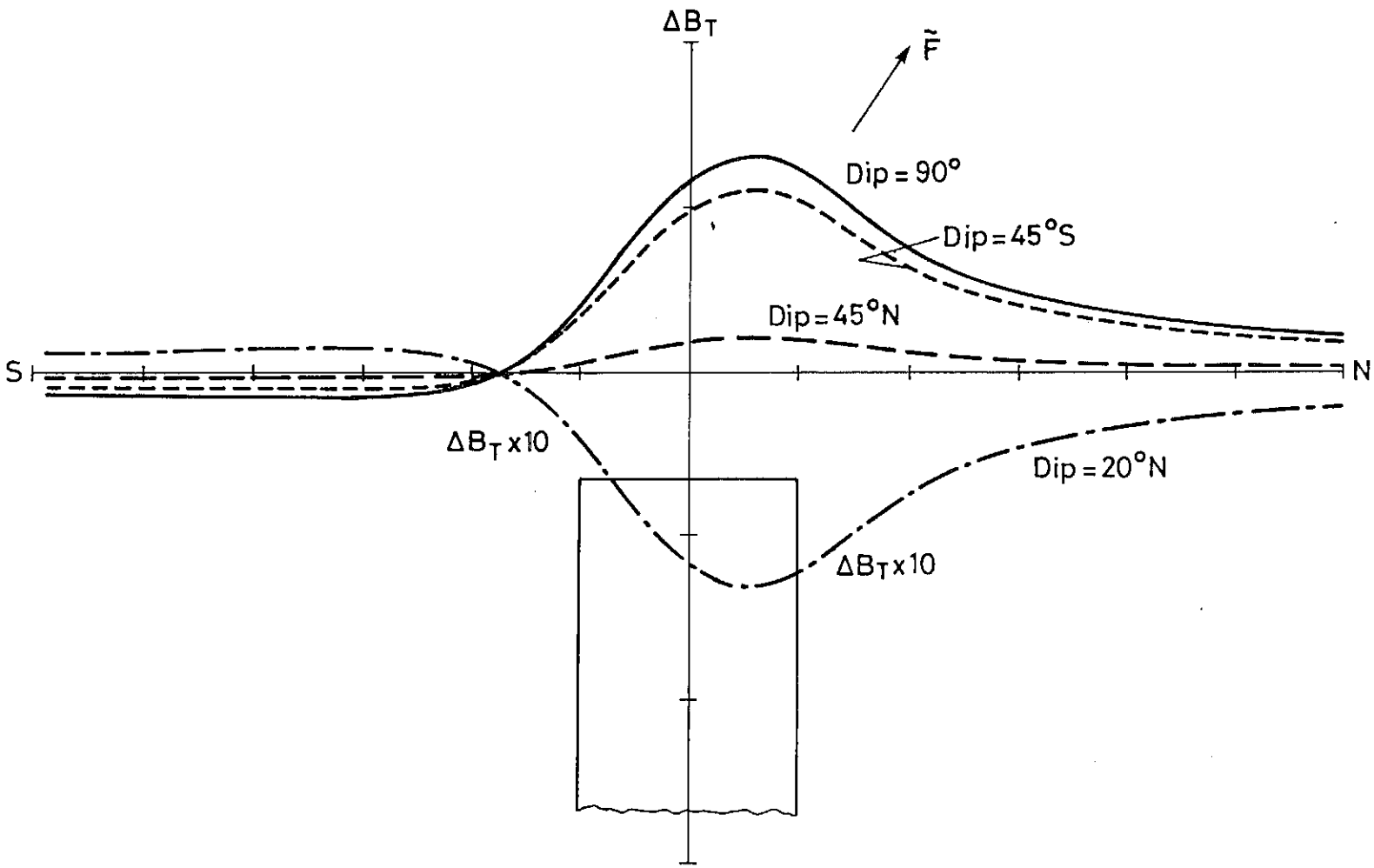

Fig. 3 . Anomaly due to the isotropic component of induced magnetisation.

ISOTROPIC DIPPING SHEETS (Q=0)

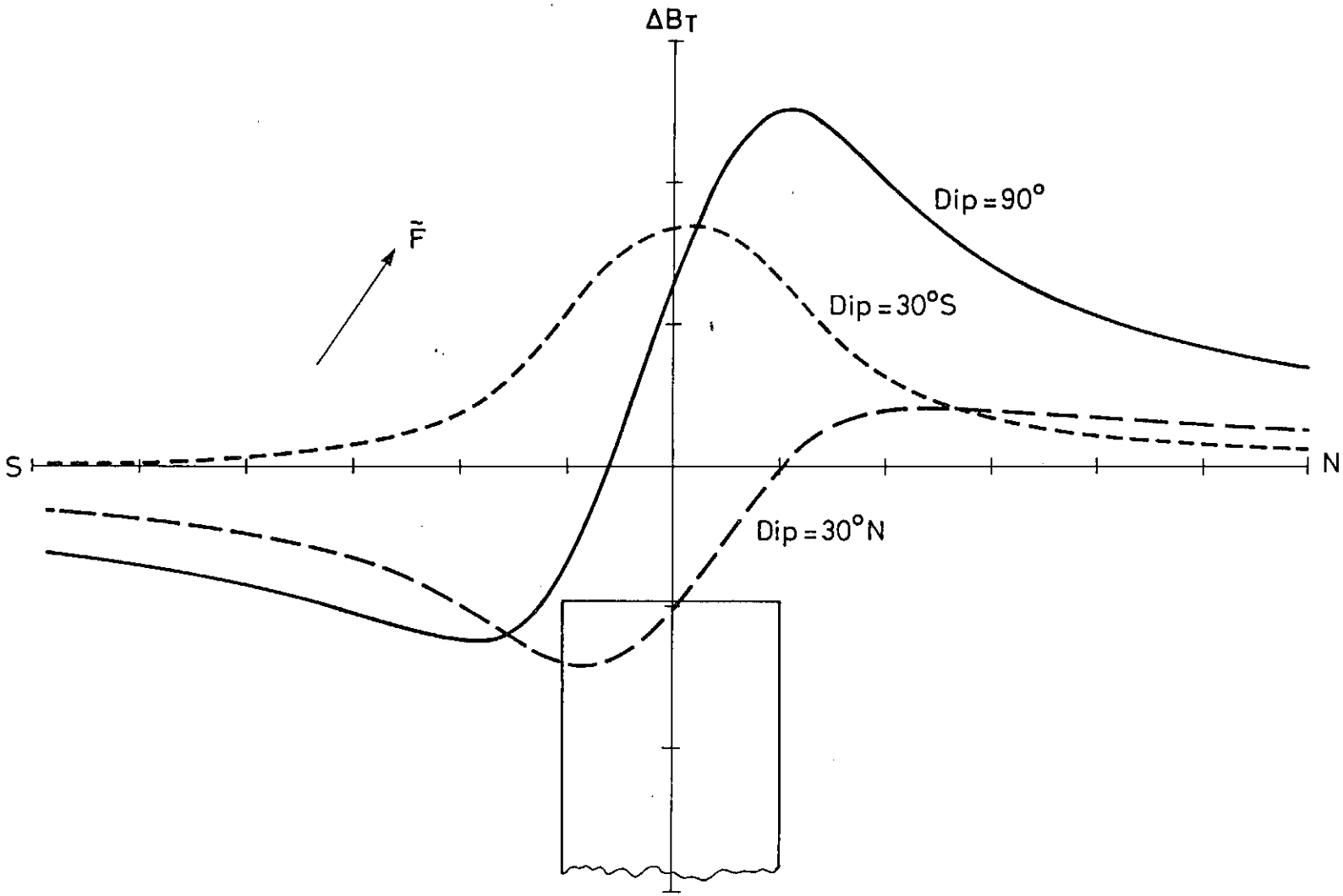

Fig. 4 . Anomaly due to post-folding remanence.

DIPPING SHEETS — POST FOLDING REMANENCE (k=0)

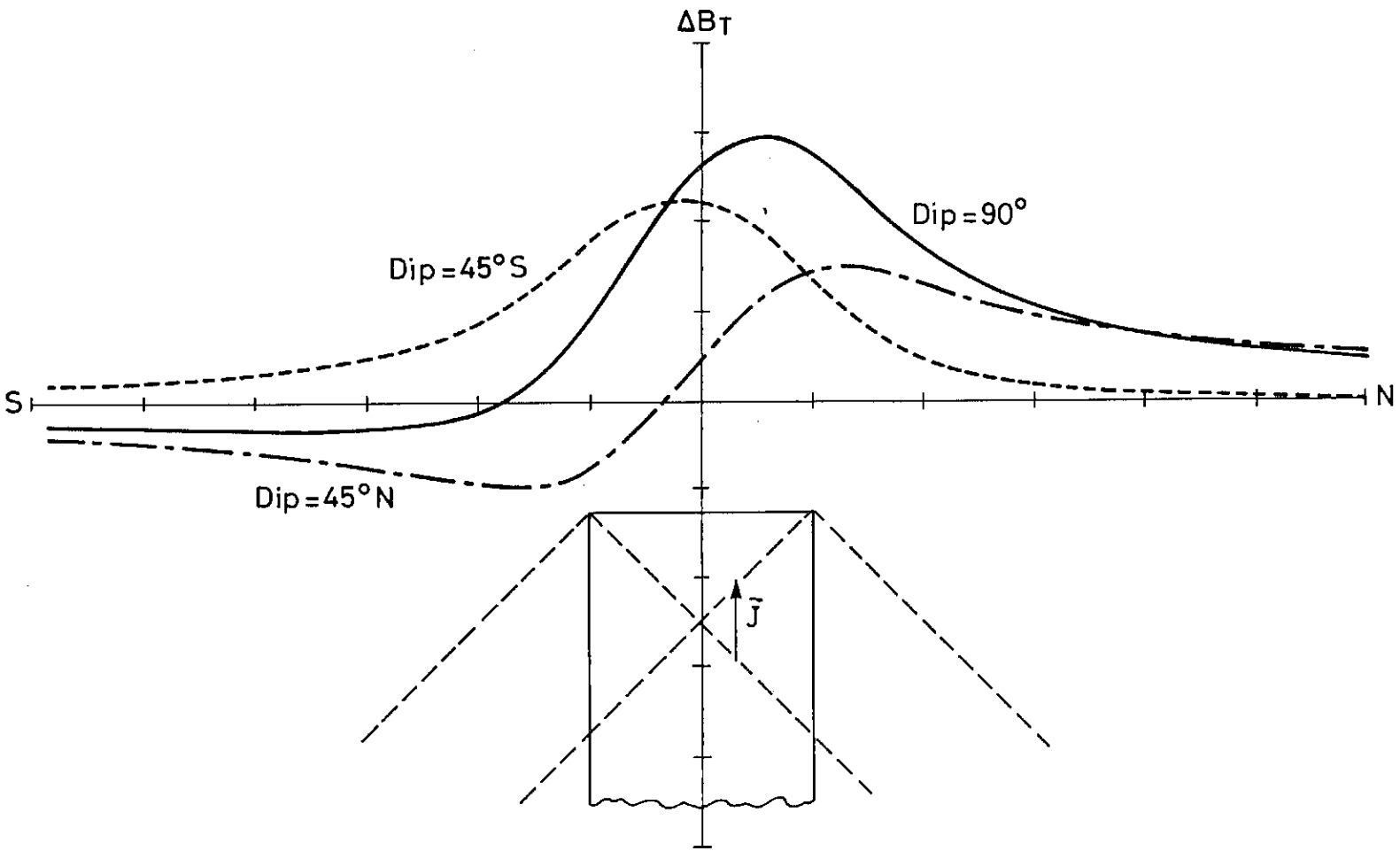

Fig. 5 . Anomaly due to pre-folding remanence over a syncline.

SYNCLINE WITH PRE-FOLDING REMANENCE (k=0)

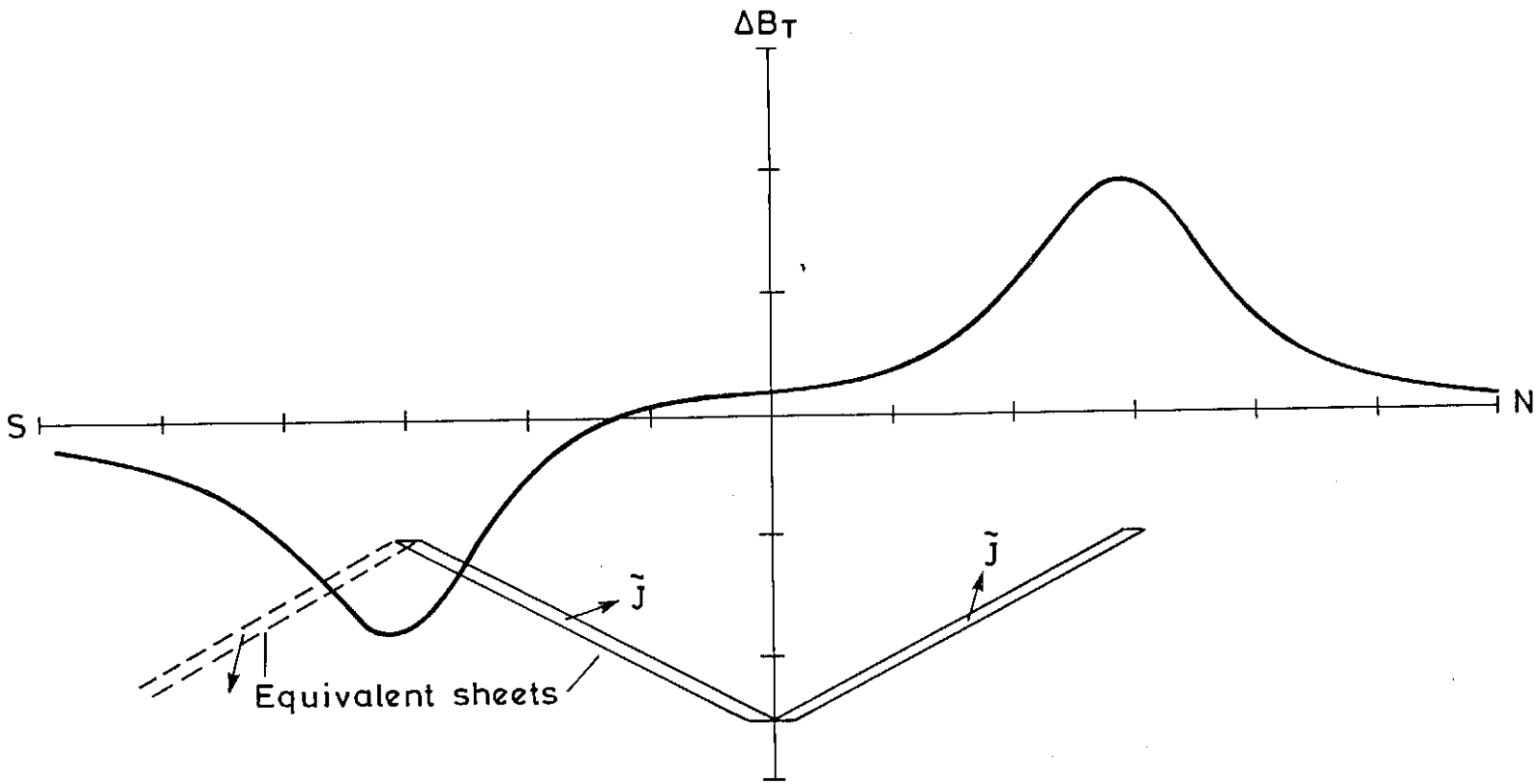

Fig. 6'. Anomalies associated with pre-folding and post-folding remanences over a thin anticlinal bed.

THIN ANTICLINAL BED ($k=0$, $D_H=0°$, $I_H=-45°$)

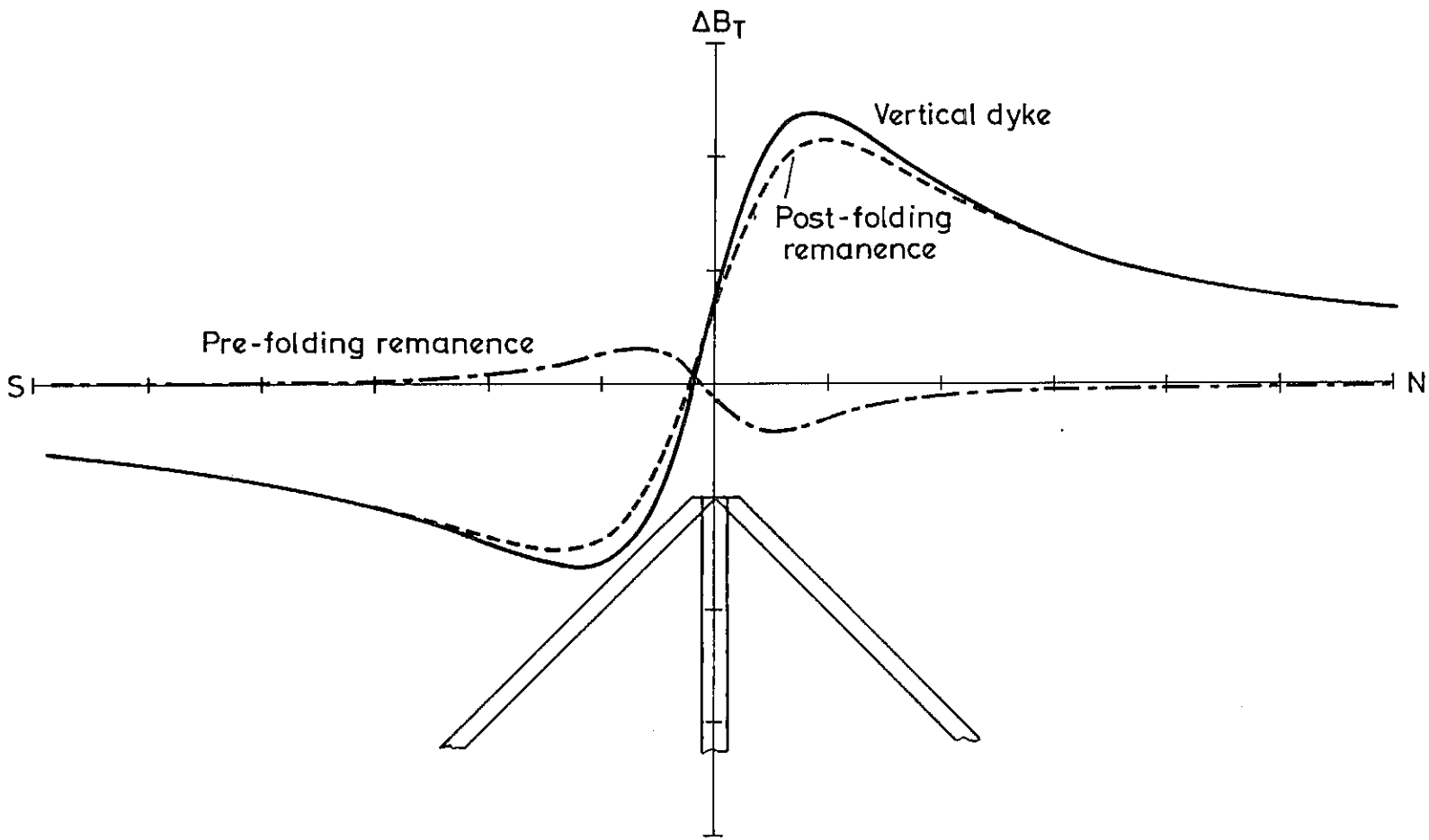

Fig. 7. Anomalies due to pre-folding and post-folding remanences over a thick anticlinal bed.

THICK ANTICLINAL BED (ERODED TOP) ($k=0$, $D_H=0°$, $I_H=-45°$)

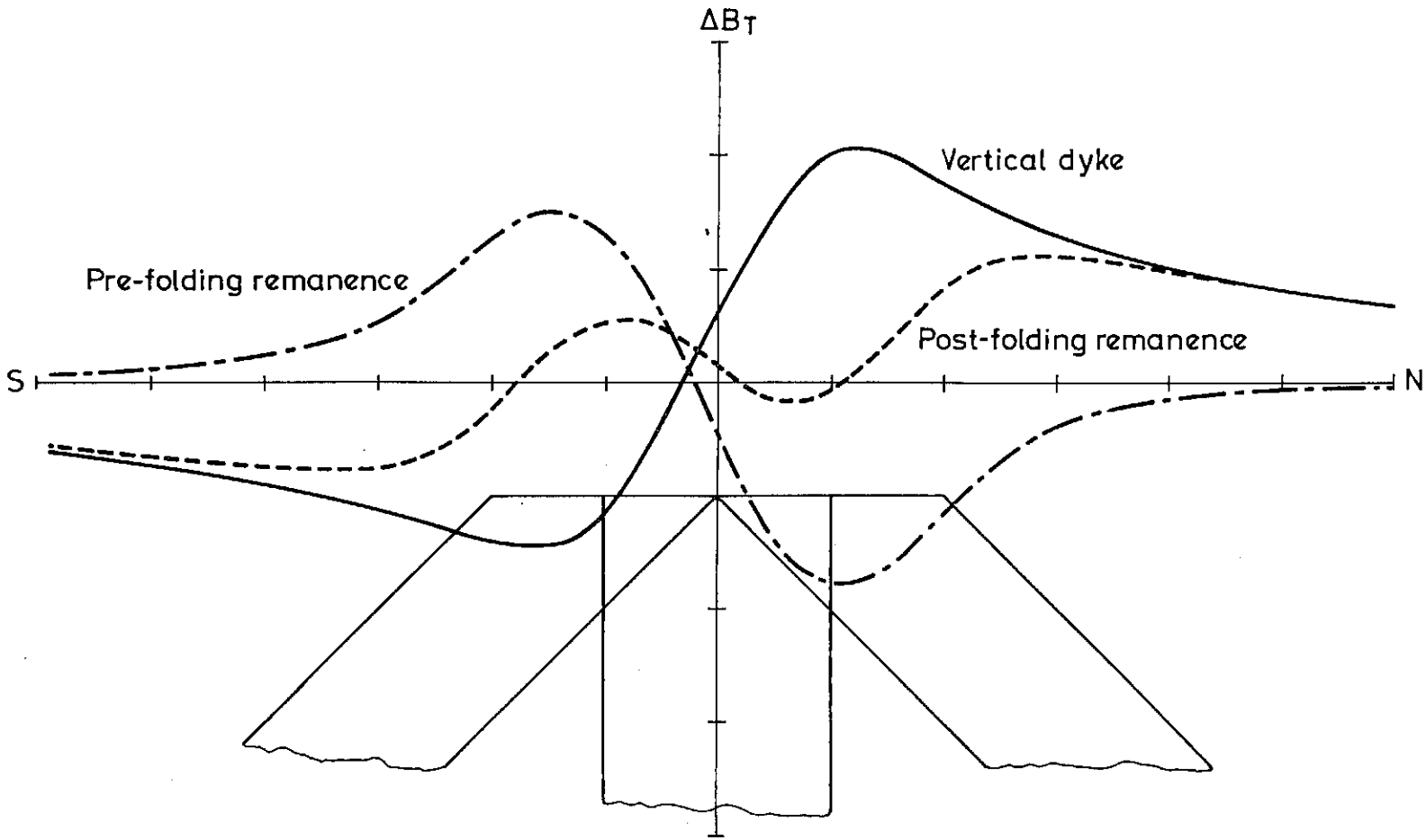

Fig. 8 : Anomaly due to anisotropic component of induced magnetisation over an anticline.

ANTICLINE WITH ERODED CREST (A=∞, Q=0)

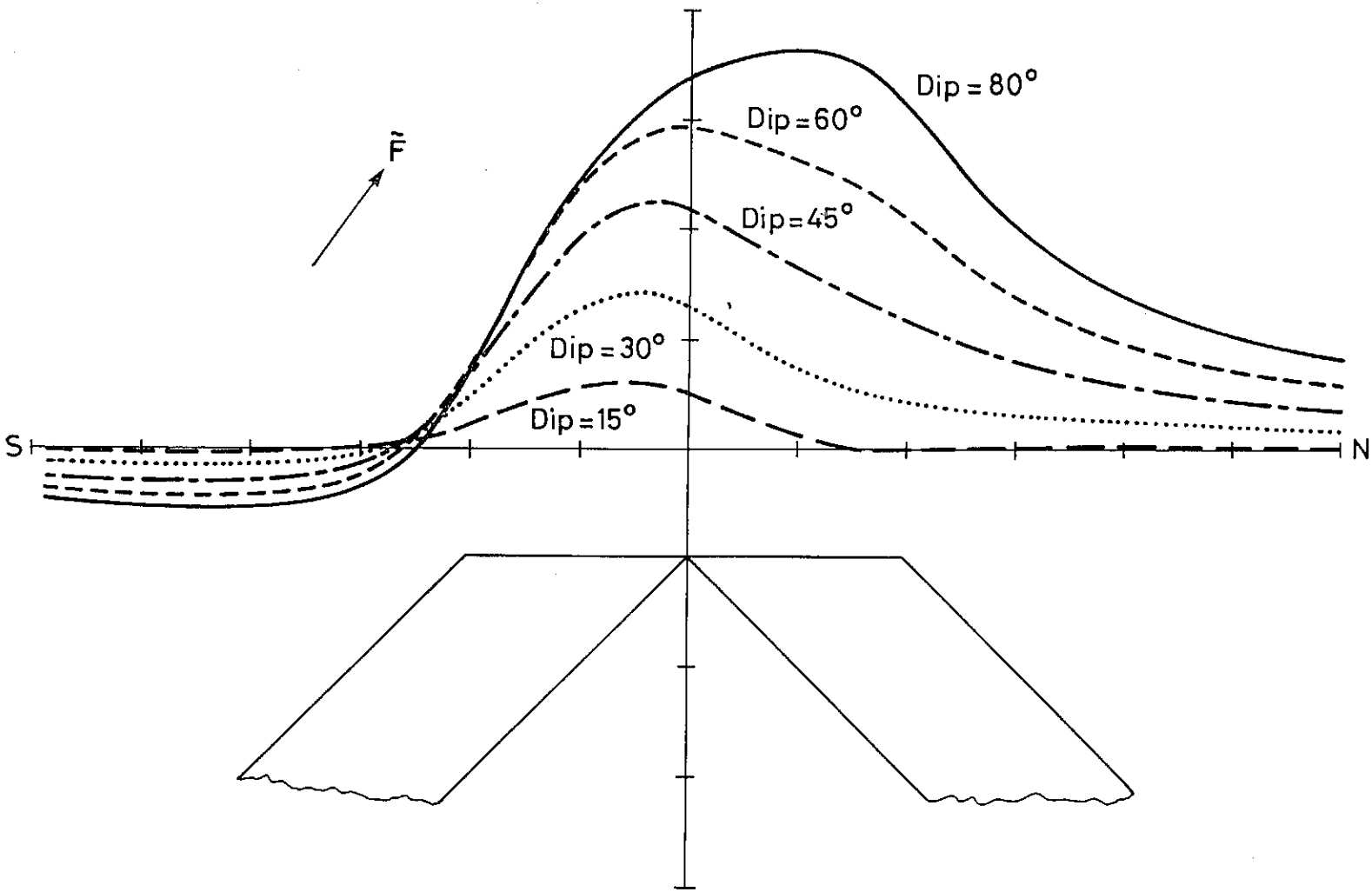

Fig. 9 Preliminary model for SW limb of Turner syncline (cf profile 1310).

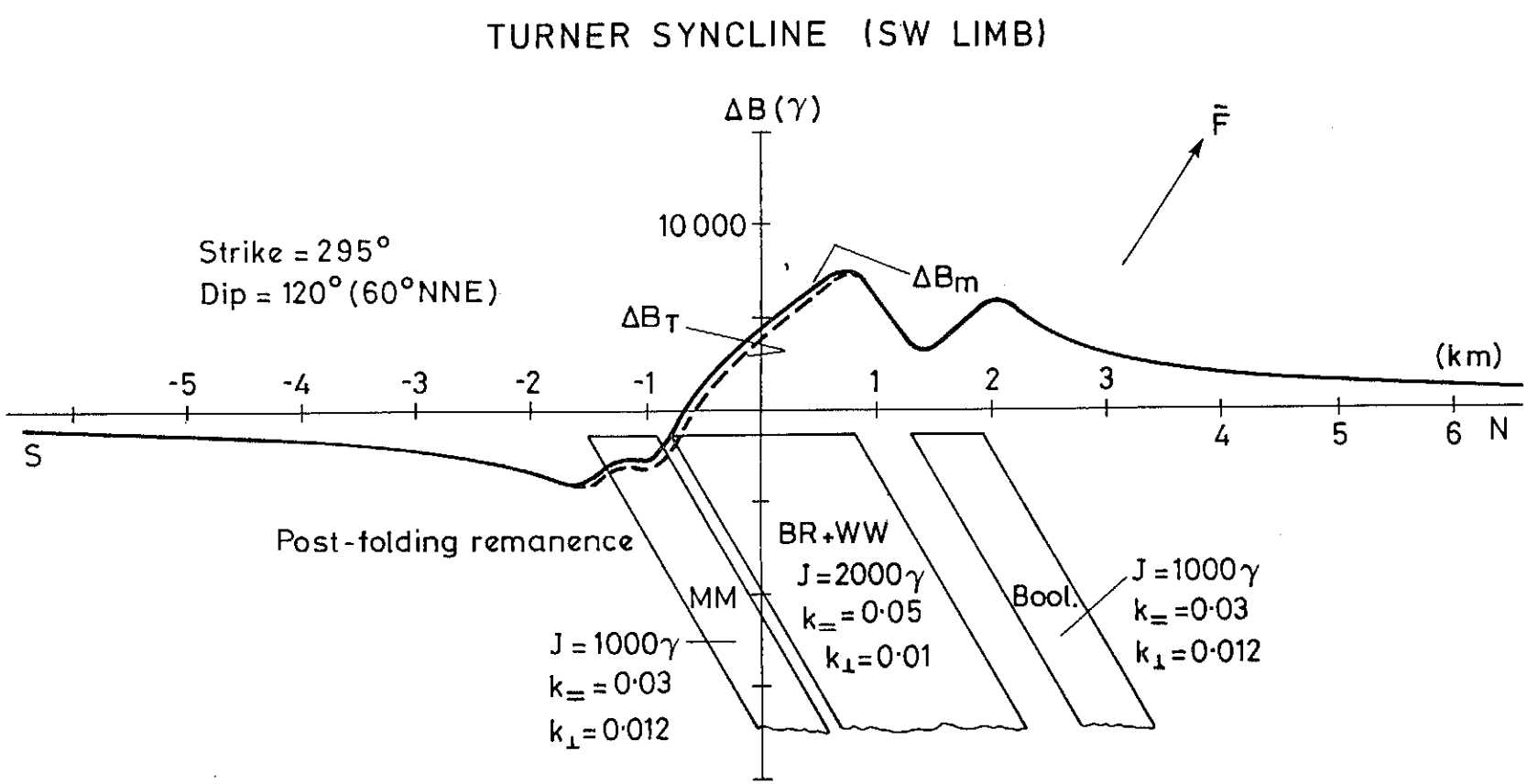
TURNER SYNCLINE (SW LIMB)
ΔB (γ)
F
10 000
Strike = 295°
Dip = 120° (60°NNE)
ΔBm
ΔBT
(km)
-5
-4
-3
-2
-1
1
2
3
4
5
6
N
S
Post-folding remanence
BR+WW
J = 2000γ
k= = 0·05
k⊥ = 0·01
MM
J = 1000γ
k= = 0·03
k⊥ = 0·012
Bool.
J = 1000γ
k= = 0·03
k⊥ = 0·012

Fig. 10 Preliminary model for SW limb of Turner syncline (cf profiles 1350 and 1400).

TURNER SYNCLINE (SW LIMB)

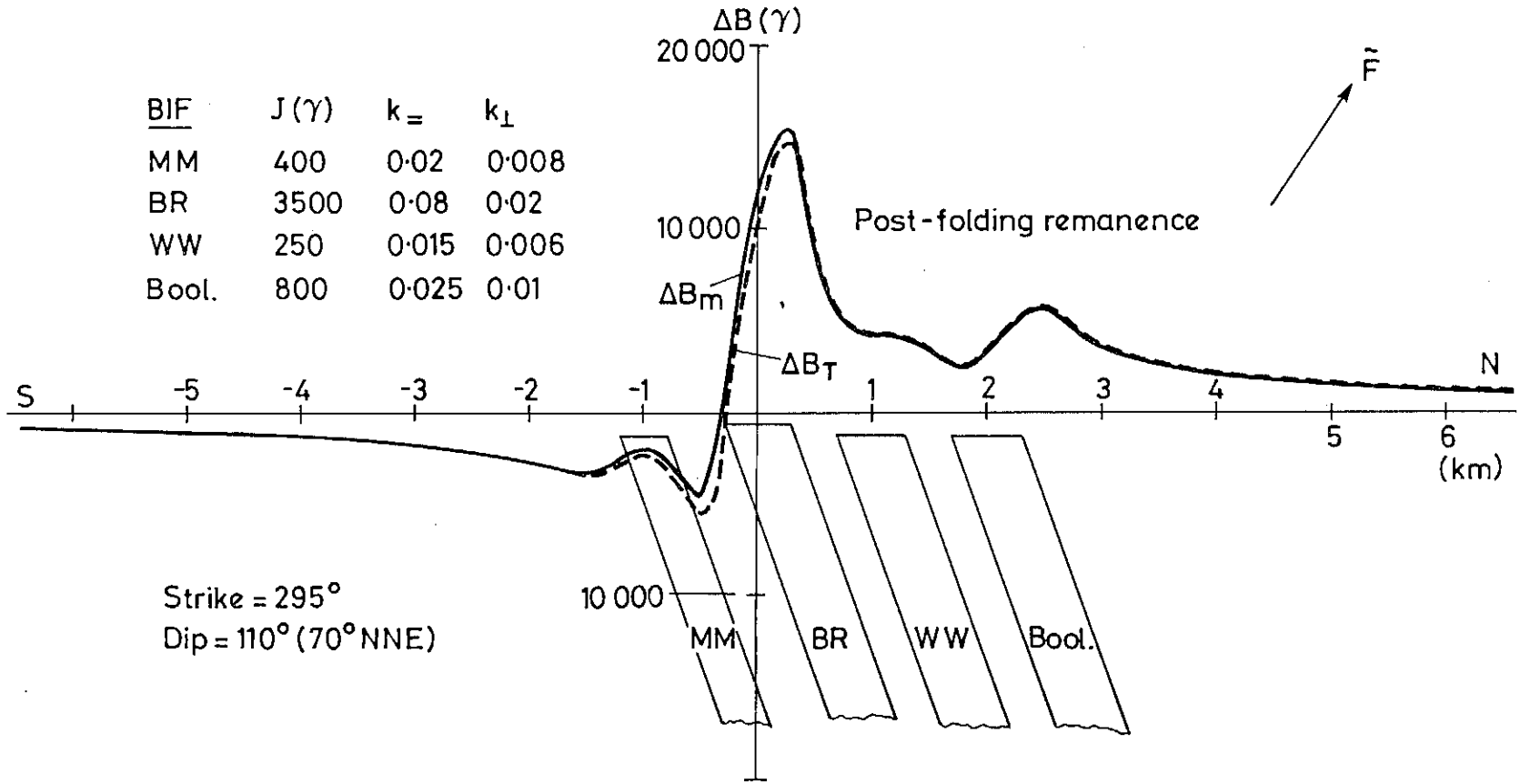

BIF	J (γ)	$k_{=}$	$k_{\perp}$
MM	400	0·02	0·008
BR	3500	0·08	0·02
WW	250	0·015	0·006
Bool.	800	0·025	0·01

Strike = 295°
Dip = 110° (70° NNE)

Fig. 11 Preliminary model for the NW limb of the Turner syncline (cf profiles 1270 and 1342).

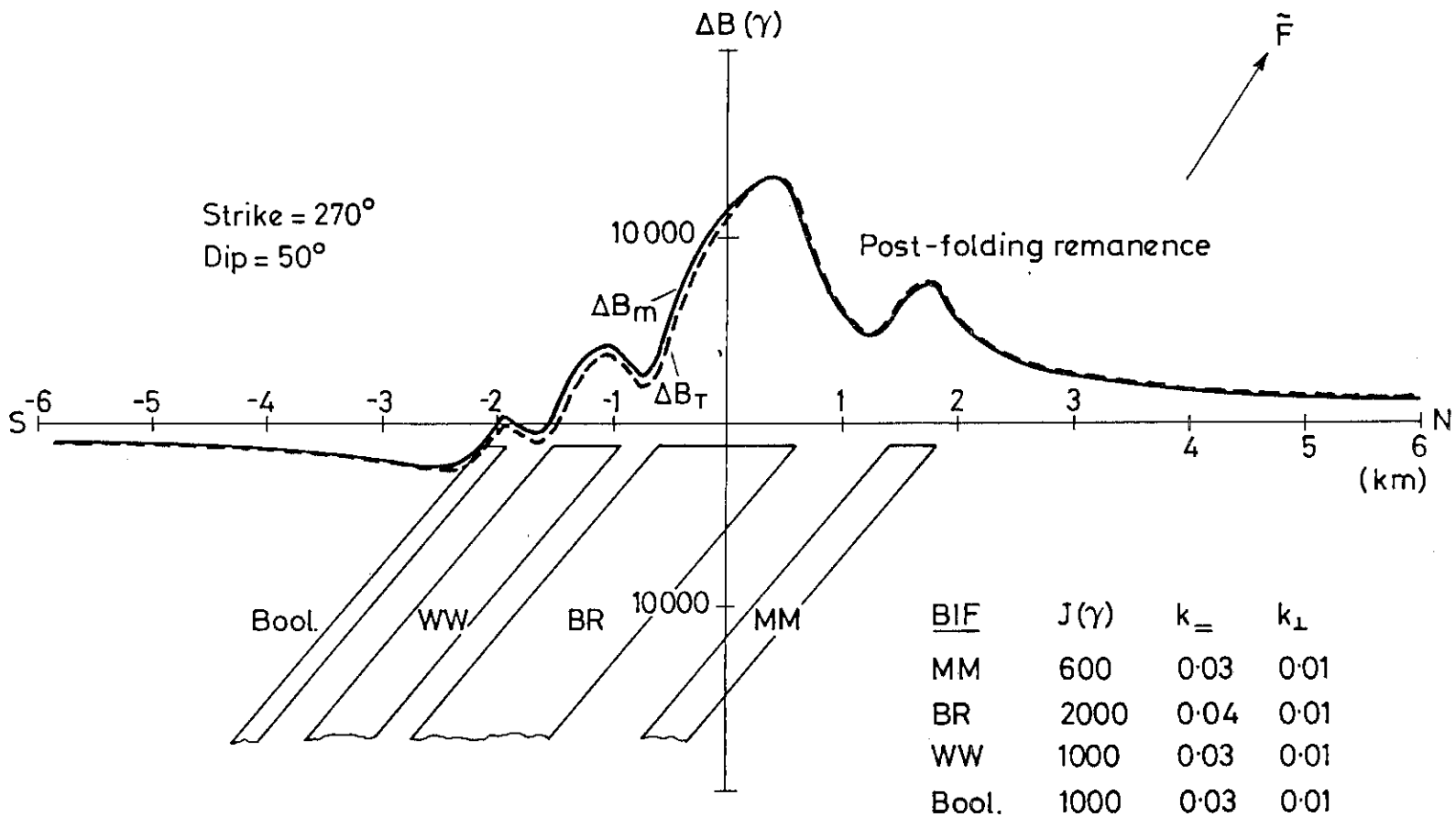

BIF	J (γ)	$k_{=}$	$k_{\perp}$
MM	600	0·03	0·01
BR	2000	0·04	0·01
WW	1000	0·03	0·01
Bool.	1000	0·03	0·01

Fig. 12 Preliminary model for the SE limb of the Turner syncline (cf profiles 1580, 1600 and 1650).

TURNER SYNCLINE (SE LIMB)